

# Effect of Chemical Structure on Polymer-Templated Growth of Graphitic Nanoribbons

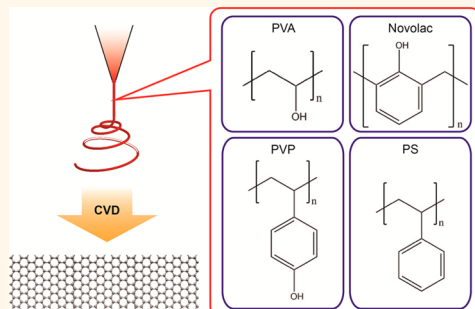
Nan Liu,<sup>†</sup> Kwanpyo Kim,<sup>†,‡</sup> Hu Young Jeong,<sup>||</sup> Po-Chun Hsu,<sup>‡</sup> Yi Cui,<sup>‡,§</sup> and Zhenan Bao<sup>\*,†</sup>

<sup>†</sup>Department of Chemical Engineering and <sup>‡</sup>Department of Materials Science and Engineering, Stanford University, Stanford, California 94305, United States,

<sup>§</sup>Stanford Institute for Materials and Energy Sciences, SLAC National Accelerator Laboratory, Menlo Park, California 94025, United States, and

<sup>||</sup>Department of Physics and <sup>||</sup>UNIST Central Research Facilities (UCRF), Ulsan National Institute of Science and Technology (UNIST), Ulsan 689-798, Korea

**ABSTRACT** Graphene nanoribbon (GNR) is an important candidate for future nanoelectronics due to its high carrier mobility and dimension-controlled band gap. Polymer-templated growth is a promising method toward high quality and massive production of GNRs. However, the obtained GNRs so far are still quite defective. In order to rationally control the crystallinity of the synthesized GNRs, herein we systematically investigate the effect of polymer chemical structure on their templated growth of GNRs. We studied the morphology/dimensions, composition, graphitization degree, and electrical conductivity of GNRs derived from four different types of electrospun polymers. The four polymers polystyrene (PS), poly(vinyl alcohol) (PVA), polyvinylphenol (PVP), and Novolac (a phenolic resin) are chosen to investigate the effect of metal binding and the effect of aromatic moieties. We found that metal-binding functional groups are crucial for obtaining uniform and continuous GNRs. On the other hand, a polymer with aromatic moieties leads to a higher  $sp^2$  percentage in the resulting GNRs, showing a higher graphitization degree and electrical conductivity.



**KEYWORDS:** graphitic nanoribbon (GraNR) · polymer · chemical structure · graphitization degree · electrospraying

Graphene is a sheet of  $sp^2$ -hybridized carbon atoms arranged into a honeycomb lattice and assembled into a two-dimensional (2D) crystal.<sup>1</sup> The exceptional electronic properties of single- and multilayer graphene, such as high conductivity, charge carrier mobility, and optical transparency,<sup>2</sup> make it an exciting material for applications in high-performance circuits,<sup>3</sup> flexible displays,<sup>4</sup> energy-storage devices,<sup>5</sup> sensors, and so on.<sup>6–8</sup> However, a 2D graphene sheet is a zero-band-gap semimetal.<sup>2</sup> The lack of a sizable band gap has limited the use of graphene in high-performance field-effect transistors (FETs) where a well-defined low-conductance (“off”) state is required for their operation.<sup>9</sup> Graphene nanoribbons (GNRs) represent a class of promising materials to tackle this challenge.<sup>10</sup> The lateral, one-dimensional confinement opens up a band gap inversely proportional to their widths, while maintaining the extraordinary transport properties of graphene.<sup>11,12</sup> For room-temperature transistor operation, it is estimated that the width of the GNRs

should be less than 30 nm.<sup>13</sup> Several methods to fabricate GNRs of widths below 50 nm have been reported. For example, GNRs can be formed by etching of graphene or carbon nanotubes (CNTs),<sup>14–16</sup> although these methods are limited in their throughput, minimal achievable width, and control of edge structures. On the other hand, GNRs can be directly synthesized from hydrocarbon molecules, on 1D metal lines or step edges of single-crystalline surfaces.<sup>13,17–20</sup> These methods, however, still cannot scalably produce GNRs with controlled width, crystallinity, and composition. Moreover, solution-phase-synthesized GNRs are typically  $\sim 2$  nm wide and several to tens of nm long. Although their atomic structure is well defined, it is difficult to directly fabricate devices due to the very short length.

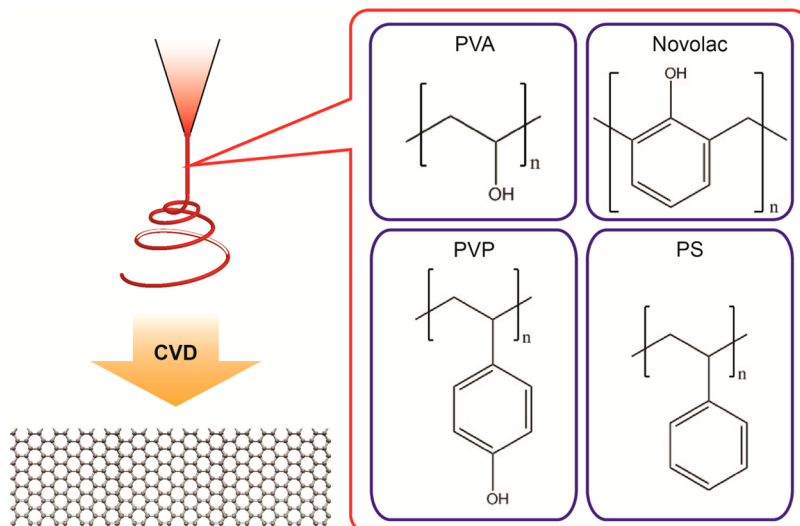
Recently, we reported a polymer-templated chemical vapor deposition (CVD) of graphitic nanoribbons (GraNRs), where metal-incorporated polymer nanofibers confine the growth of 1D graphitic structures.<sup>21,22</sup> Compared to other 1D templates such as metal nanobars,

\* Address correspondence to zbao@stanford.edu.

Received for review May 24, 2015 and accepted August 12, 2015.

Published online August 12, 2015  
10.1021/acsnano.5b03134

© 2015 American Chemical Society



**Scheme 1.** CVD growth of GraNRs from a variety of electrospun polymers. Chemical structures of PVA, Novolac, PVP, and PS are on the right of the panel.

the polymer nanofibers produce much longer and more uniform GraNRs. We hypothesized that polymer binding with metal ions is important to stabilize the ions at elevated temperatures. Moreover, the polymer nanofibers can be formed by solution-based processes such as electrospinning, thus substantially enhancing the throughput and scalability.

A further understanding of polymer-templated growth of GraNRs requires an in-depth understanding of the influence of different parameters, as well as the growth mechanism. The chemical structure of the polymer templates may play a critical role in the CVD synthesis of GraNRs. On one hand, polymer–metal interaction may help to stabilize the metal catalyst from aggregation and may affect the effectiveness of the 1D confinement. On the other hand, the polymer serves as a carbon source alongside extraneous precursors (*e.g.*, methane). As a result, its chemical structure, in particular the degree of  $sp^2$  hybridization, can affect the graphitization degree of the resultant GraNRs. Therefore, the investigations of different polymer templates thus can shed light on the growth mechanism of GNRs and potentially improve their qualities. This, however, has largely been unexplored.

In this work, we aim at answering the question of how the chemical structure of polymer templates affects the GraNR growth. With further understanding and development, it is foreseeable that the crystalline domain size and atomic structures may be controlled at designated locations, which is our long-term goal. However, understanding the growth mechanism and the correlation between the quality of GraNRs and the polymers' chemical structures for future polymer design is the main objective of this paper.

In this work, we utilize electrospun polymer nanofibers from various chemical structures for the templated CVD synthesis of GraNRs, in order to understand

the growth mechanism as well as to rationally control the GraNRs' crystallinity. Specifically, we focus on two aspects of the polymer chemical structures, *i.e.*, metal-binding functional groups and aromatic moieties. Four types of polymers are investigated: polystyrene (PS), poly(vinyl alcohol) (PVA), polyvinylphenol (PVP), and Novolac phenolic resin (Scheme 1). Detailed characterizations were carried out to elucidate the effect of these different polymers on the morphology, composition, atomic structure, and electrical properties of the resultant GraNRs. We found that the presence of a metal-binding functional group is indeed crucial for the formation of uniform and continuous ribbons. Moreover, polymers with more aromatic moieties can lead to a higher graphitization degree, corresponding to a higher  $sp^2$  carbon percentage, higher electrical conductivity, and larger graphitic domain sizes. We believe these findings provide important insights on the growth mechanism of polymer-templated GNRs and provide guidelines for the design of new polymers for future improvement of the quality of GNRs.

## RESULTS AND DISCUSSION

Electrospinning is a powerful tool to create polymer nanostructures.<sup>23–25</sup> In our case, all four polymers can be electrospun into nanofibers with *ca.* 100 nm diameter (Figure S1). Among the four polymers, PVA, PVP, and Novolac have hydroxyl groups that can bind with metal cations, while PS does not have such functional groups. This allows us to observe the effect of metal–polymer interaction on GNR growth. From another perspective, PVA consists solely of  $sp^3$ -hybridized carbon in its backbone, while PVP and Novolac both have one benzene ring in each repeating unit. This contrast allows for a comparative study of the effect of benzene rings on the graphitization and crystallinity of the resultant GNRs.

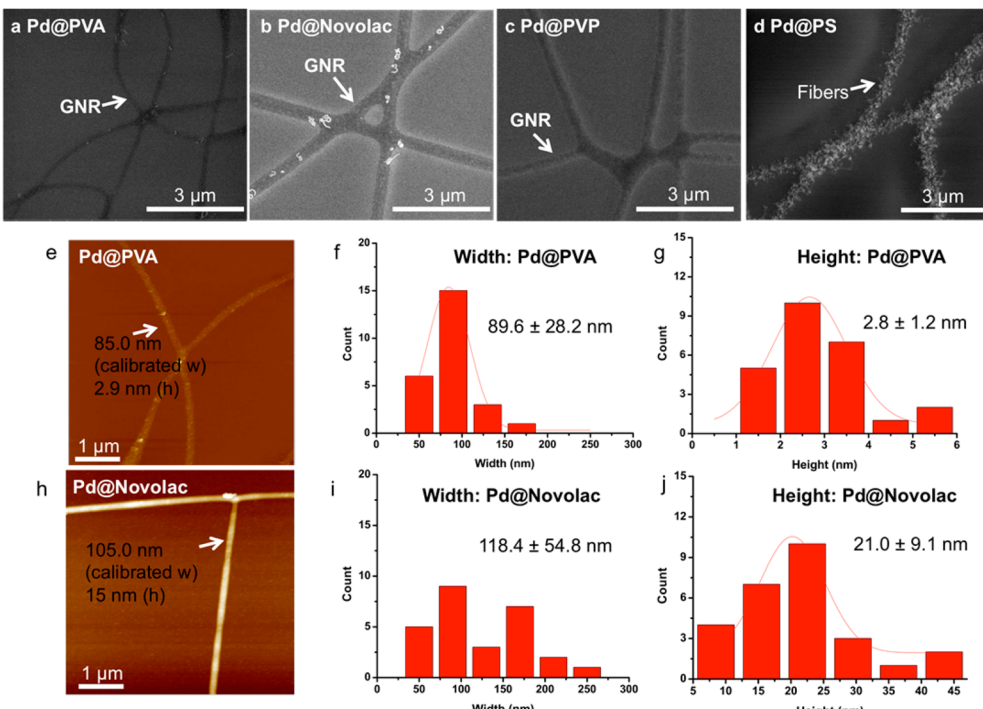


**Figure 1.** Mophology of the GNRs. SEM images of carbon structures grown from Pd@PVA (a), Pd@Novolac (b), Pd@PVP (c), and Pd@PS (d). AFM images of GNRs from Pd@PVA (e) and Pd@Novolac (h) nanofibers and their corresponding width (f, i) and height (g, j) histograms.

Next, we performed low-pressure CVD growth on the Pd-incorporated polymer nanofibers at typical conditions (see Supporting Information, Figure S1). SEM and AFM were used to monitor the morphology changes from polymer nanofibers to postgrowth nanoribbons. From the SEM micrographs, we observed that 1D ribbon-like structures were formed from PVA, PVP, and Novolac templates (Figure 1a, b, and c). The widths of the ribbons are quite uniform along their axial directions. To further investigate the correlation between the dimensions of the polymer nanofibers and their corresponding postgrowth nanoribbons, we performed systematic AFM characterizations (Figure S2 and Figure 1e–j). The AFM tip convolution effect was corrected in the width measurement. These three polymer nanofibers (PVA, PVP, and Novolac) exhibit similar widths and heights around 100 nm, with isotropic cross sections. After CVD growth, the dimensions of the nanoribbons are obviously smaller. The average widths of nanoribbons derived from PVA, Novolac, and PVP decreased by about 14%, 16%, and 40%, respectively, compared to that of the starting nanofibers. The heights decreased by about 97%, 84%, and 90%, respectively. This reduction in size originates from the high-temperature vaporization and graphitization of the polymer templates. It is noted that the average widths of PVA- and PVP-postgrowth structures both fall into the range of sub-90 nm, and some of the ribbons are as small as 30 nm, which are suitable for room-temperature field-effect-transistor operation.<sup>13</sup> On the

other hand, we also note that the average height for each type of polymer postgrowth ribbon is very small (3–20 nm). This anisotropic shrinkage is possibly due to the inhomogeneous temperature distribution above the heated substrate. During the CVD process, the polymer near the surface may have vaporized faster. The average height of PVA-derived ribbons is the smallest (~2.8 nm), which may be related to the lowest vaporization/graphitization temperature of this particular polymer among the three. In contrast, the Novolac-derived ribbons are much thicker (~21 nm on average), which fall into the category of graphitic nanoribbons. These observations clearly show that the polymer type greatly affects the morphology and dimensions of the postgrowth nanoribbons.

The postgrowth structure from the PS template (Figure 1d) shows a drastically different structure from the three polymers discussed above. The starting 1D templates collapsed, giving rise to a large quantity of fibers that protruded out of the original template. As a result, no nanoribbon structures could be resolved. We note that PS does not have hydroxyl groups that interact with Pd<sup>2+</sup> like the other three polymers. This may have led to more severe agglomeration and deactivation of the metal catalyst at elevated temperatures. To test this hypothesis, we heated Pd@PVP and Pd@PS polymer fibers to 500 °C in H<sub>2</sub> without carrying out the CVD growth. As shown in Figure 2, Pd@PVP nanofibers after annealing retained the fiber morphology, but the Pd@PS nanofibers broke down into agglomerates.

These results indicate that polymer templates with stronger metal-binding sites improve the graphitization degree of the resulting nanoribbons, providing an efficient method to obtain high-quality GNRs.

Next, we explore the effect of having benzene moieties on the graphitization degree of the nanoribbons. X-ray photoelectron spectroscopy (XPS) of the C 1s core level is sensitive to the bonding configuration of the carbon atoms.<sup>26</sup> We took C 1s XPS spectra of Pd-incorporated PVA, Novolac, and PVP polymer fibers on SiO<sub>2</sub>/Si substrates as well as their respective post-growth nanoribbons (Figure 3). The same Pd<sup>2+</sup> concentrations were used in their electrospinning solutions (20 mg/mL). The baseline-subtracted XPS spectra were analyzed using a fitting routine to deconvolute each spectrum into individual Gaussian–Lorentzian peaks. The percentage of sp<sup>2</sup> carbon was determined by the area of the peak centered at 284.1 eV with a full width at half-maximum (fwhm) of 1.2 eV.<sup>27</sup> The percentage of sp<sup>3</sup> carbon was quantified by the peak centered at 285.0–285.5 eV with variable peak width.<sup>27</sup> Other peaks corresponding to carbide and C–O were also fitted. The peak assignments and percentage of each carbon species can be found in Table S1 and Figure S3.

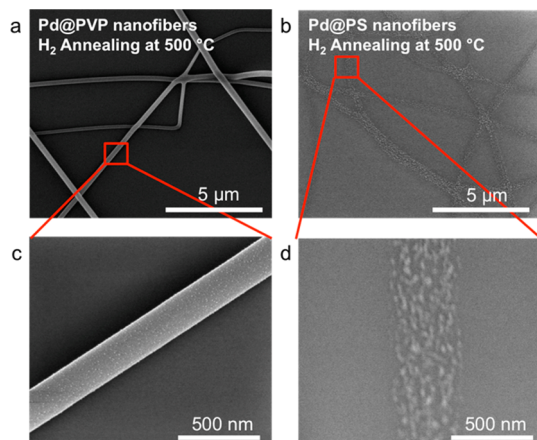


**Figure 2.** SEM images of Pd@PVP (a, c) and Pd@PS (b, d) nanofibers after annealing in H<sub>2</sub> at 500 °C. (c, d) Zoom-in images of the red square regions in (a) and (b).

The percentage of sp<sup>2</sup> carbon in the postgrowth nanoribbons from Pd@PVA, Novolac, and PVP templates is 55%, 71%, and 82%, respectively. Interestingly, there is a positive correlation between the sp<sup>2</sup> carbon content in the postgrowth nanoribbons and that in their respective polymer templates. This correlation suggests that the composition of postgrowth nanoribbons is highly dependent on their nanofiber templates. The benzene moieties in the polymer templates presumably provide nucleation centers for the growth of graphitic domains during CVD, thus enhancing the sp<sup>2</sup> carbon content. This observation provides a viable route to tune the graphitization degree of polymer-templated GNRs.

To evaluate the graphitic domain sizes of the post-growth nanoribbons and correlate them with the nature of the polymer templates, we carried out high-resolution TEM observations of GraNRs grown from electrospun Pd@PVA, Pd@Novolac, and Pd@PVP fibers. Figure 4a–c shows the atomic-resolution images. Their corresponding FFT (fast Fourier transform) patterns were used to compare the graphitization degree (Figure S4). The average graphitic domain size can be evaluated from the fwhm of the first peak corresponding to the (100) lattice plane of graphene in the radially integrated FFT pattern. According to the Scherrer equation, the domain size is inversely proportional to the broadening (fwhm) of the scattering vector in reciprocal space.<sup>28–30</sup> The GNR from Pd@PVP shows the narrowest peaks, indicating the largest average graphitic domain size among the three types of polymer. We also conducted electron diffraction characterization on those GraNRs, which can identify the graphitization degree over a relatively large area. Again, from the scattering vector in the reciprocal space, graphitic domain sizes of the nanoribbons fall in the sequence of Pd@PVP, Pd@Novolac, and Pd@PVA. This is consistent with our XPS study, confirming that polymer containing a higher sp<sup>2</sup> percentage will result in a higher graphitization degree.

Raman spectroscopy was conducted to analyze the crystallite size.<sup>31</sup> Figure 5a shows the typical

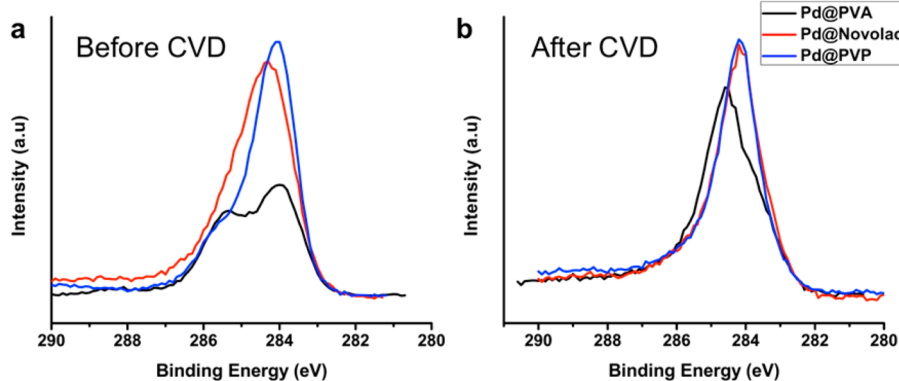


**Figure 3.** C 1s XPS spectra of Pd@PVA, Pd@Novolac, and Pd@PVP nanofibers before (a) and after (b) CVD growth.

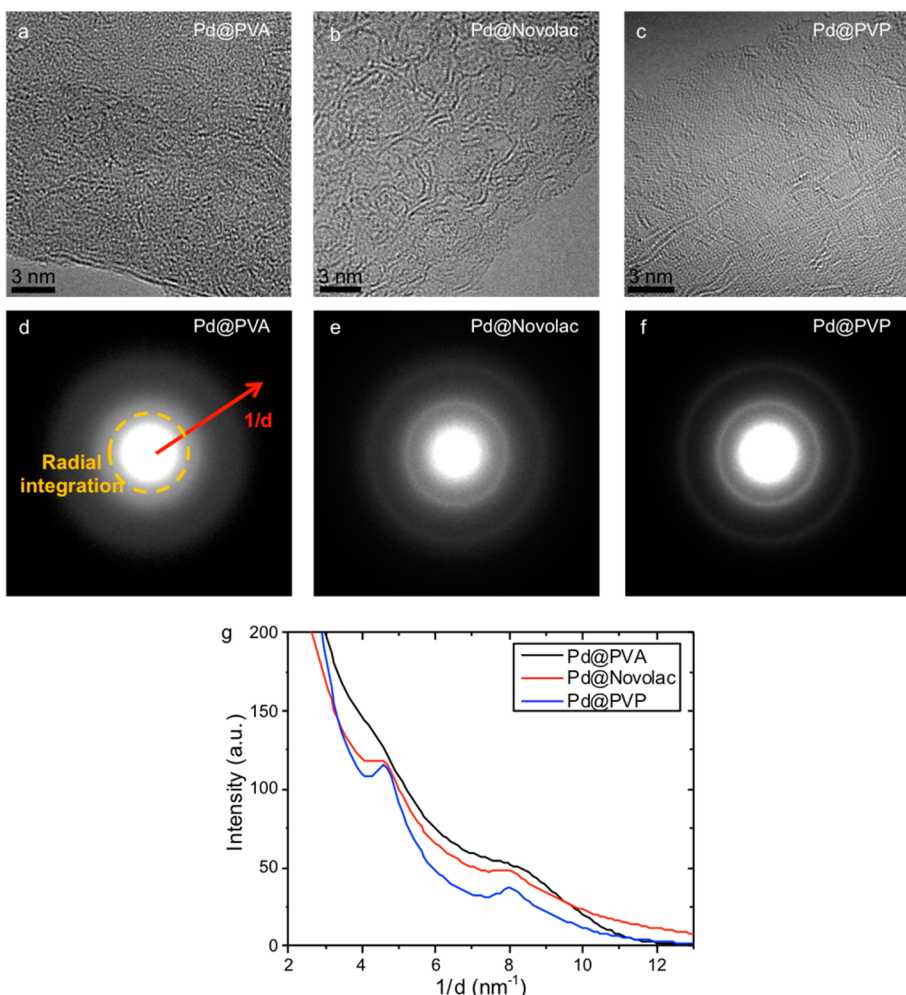


**Figure 4.** Atomic-resolution TEM images (a, b, c) and corresponding electron diffraction patterns (d, e, f) of GraNRs grown from electrospun Pd@PVA (a, d), Pd@Novolac (b, e), and Pd@PVP (c, f). (g) Intensity profiles of the electron patterns integrated along the radial direction.

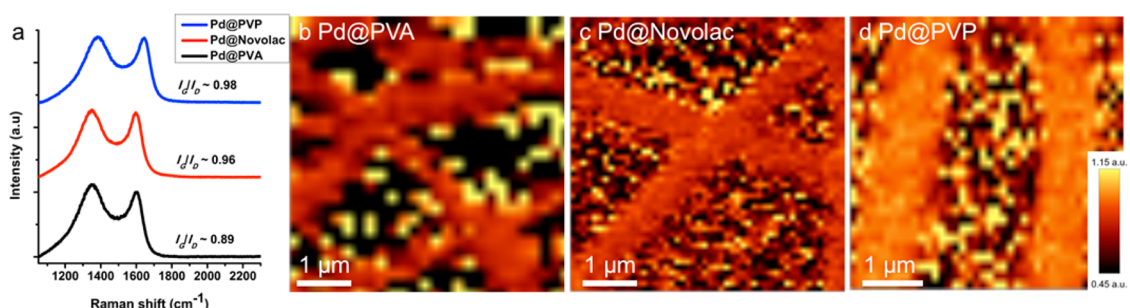


**Figure 5.** (a) Raman spectra of GraNRs grown from Pd@PVA (black), Pd@Novolac (red), and Pd@PVP (blue). (b, c, d) Raman mappings of  $I(G)/I(D)$  over several ribbons with the same color scale.

Raman spectra of nanoribbons grown from Pd@PVA, Pd@Novolac, and Pd@PVP. The crystallite size can be estimated from the intensity ratio of the D to G peak following the Tuinstra–Koenig equation.<sup>32,33</sup> We did Raman mapping over several GNRs from Pd@PVA, Pd@Novolac, and Pd@PVP and plotted their peak intensity ratio ( $I_G/I_D$ ) maps using the same color scale (Figure 5b, c and d). GraNRs from Pd@PVP show the brightest contrast along the ribbons, indicating the

biggest domain size. Together with our TEM observations, we confirmed that polymer having a higher portion of benzene moieties will lead to GraNRs with a higher graphitization degree.

We further test the conductivity of the postgrowth nanoribbons. The conductivity of one-dimensional carbon nanostructures is a direct indicator of their quality and crystallinity.<sup>34,35</sup> First, we electrospun nanofibers at low density on quartz substrates and performed CVD

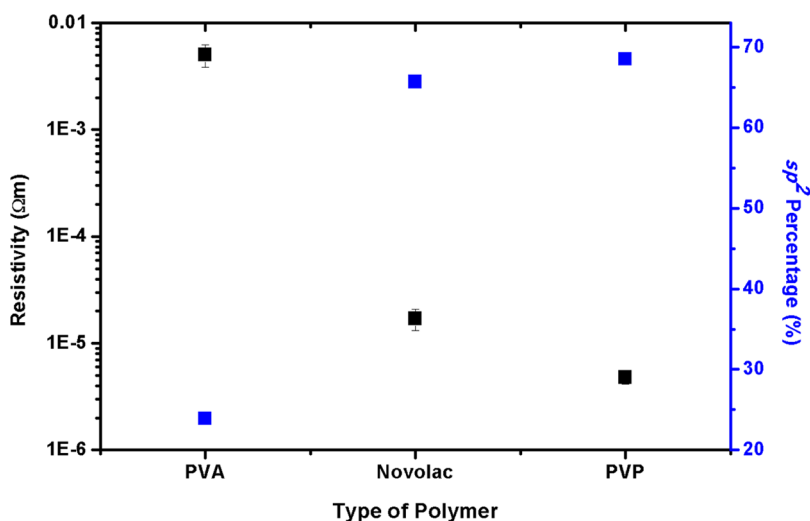


**Figure 6.** Polymer type dependence on the resistivity (left vertical axis) of postgrowth nanoribbons. Right vertical axis exhibits their corresponding  $\text{sp}^2$  carbon percentage in the polymer templates.

growth at typical conditions. Then, metal contact (Ti/Pd) arrays were deposited on the postgrowth substrate using a photolithography mask. We specifically chose the devices with individual GraNRs crossing multiple ( $\geq 4$ ) electrodes and measured their four-probe resistances. The following formula was used to calculate the resistivity ( $\rho$ ):

$$\rho = R \frac{wd}{l}$$

where  $w$ ,  $d$ , and  $l$  are the width, height, and length of the measured ribbon, respectively. For each type of polymer, we tested five single-ribbon devices. Their conductivity and respective concentrations of  $\text{sp}^2$  carbon are summarized in Figure 6. Consistent with the XPS study, the postgrowth nanoribbon from Pd@PVA shows the highest resistivity, more than 2 orders of magnitude larger than nanoribbons from Pd@Novolac and PVP. The resistivities of GNRs from Pd@PVP are slightly smaller than those from Pd@Novolac. This conductivity dependence further confirms the hypothesis that a higher  $\text{sp}^2$  carbon ratio in the polymer

templates will lead to a higher graphitization degree in the resulting nanoribbons. This provides a guideline for choosing polymer templates for the synthesis of higher quality GNRs.

## CONCLUSIONS

In conclusion, in order to rationally control the crystallinity of the GraNRs, we systematically investigated the effect of chemical structures on polymer-templated GraNR growth. We chose four types of polymer (PS, PVA, Novolac, and PVP) to specifically understand the role of metal-binding functional groups and benzene moieties. It is found that a metal-binding functional group is indeed important for the formation of uniform and continuous ribbons. Polymer with more benzene moieties is crucial for improving the graphitization degree and electrical conductivity in the resultant ribbons. These understandings shed important light on the growth mechanism of polymer-templated GNRs and provide guidelines for the design of new polymers for further improvement of the quality of GNRs.

## METHODS

**Synthesis of GraNRs.** The electrospinning technique was used to produce polymer nanofiber templates. The Pd@PVA, Pd@PVP, and Pd@PS nanofibers were electrospun from water, tetrahydrofuran (THF), and methyl ethyl ketone (MEK) solutions, respectively, with  $\text{Pd}(\text{OAc})_2$  and myristyl trimethylammonium bromide (MTMAB) additives. Pd@Novolac nanofibers were electrospun from commercially available photoresist (SPR 220-7). The growth of GraNRs was performed in a low-pressure thermal CVD system with methane and hydrogen as the carbon source and carrier gas, respectively. Details of the experimental methods can be found in the Supporting Information.

**Characterizations.** The morphology of the polymer nanofibers and as-grown GraNRs were studied by scanning electron microscopy (SEM) (Magellan system (FEI)) and atomic force

microscopy (AFM, Nanoscope-III, Digital Instrument). Dimensions of the GraNRs were measured in tapping mode AFM. The convolution effect of the AFM tip was calibrated using a carbon nanotube sample. Raman spectra were taken on a confocal Raman system (WITec 500) using 532 nm laser excitation. X-ray photoelectron spectroscopy was carried out with a PHI 5000 Versaprobe equipped with a monochromatic Al K source. Room-temperature four-probe conductivity was measured on a probe station with a semiconductor analyzer (Keithley 4200-SCS).

**Conflict of Interest:** The authors declare no competing financial interest.

**Acknowledgment.** This work was funded by Stanford Global Climate and Energy Project (GCEP).

*Supporting Information Available:* The Supporting Information is available free of charge on the ACS Publications website at DOI: 10.1021/acsnano.5b03134.

Experimental details and additional figures (PDF)

## REFERENCES AND NOTES

- Novoselov, K. S.; Geim, A. K.; Morozov, S. V.; Jiang, D.; Zhang, Y.; Dubonos, S. V.; Grigorieva, I. V.; Firsov, A. A. Electric Field Effect in Atomically Thin Carbon Films. *Science* **2004**, *306*, 666–669.
- Geim, A. K.; Novoselov, K. S. The Rise of Graphene. *Nat. Mater.* **2007**, *6*, 183–191.
- Lin, Y.-M.; Dimitrakopoulos, C.; Jenkins, K. A.; Farmer, D. B.; Chiu, H.-Y.; Grill, A.; Avouris, P. 100-GHz Transistors from Wafer-Scale Epitaxial Graphene. *Science* **2010**, *327*, 662.
- Bae, S.; Kim, H.; Lee, Y.; Xu, X.; Park, J.-S.; Zheng, Y.; Balakrishnan, J.; Lei, T.; Kim, H. R.; Song, Y. I., Roll-to-Roll Production of 30-in. Graphene Films for Transparent Electrodes. *Nat. Nanotechnol.* **2010**, *5*, 574–578.
- Stoller, M. D.; Park, S.; Zhu, Y.; An, J.; Ruoff, R. S. Graphene-Based Ultracapacitors. *Nano Lett.* **2008**, *8*, 3498–3502.
- Xia, F.; Mueller, T.; Lin, Y.-m.; Valdes-Garcia, A.; Avouris, P. Ultrafast Graphene Photodetector. *Nat. Nanotechnol.* **2009**, *4*, 839–843.
- Liu, N.; Tian, H.; Schwartz, G.; Tok, J. B.-H.; Ren, T.-L.; Bao, Z. Large-area, Transparent, and Flexible Infrared Photodetector Fabricated Using pn Junctions Formed by n-doping Chemical Vapor Deposition Grown Graphene. *Nano Lett.* **2014**, *14*, 3702–3708.
- Novoselov, K. S.; Fal'ko, V.; Colombo, L.; Gellert, P.; Schwab, M.; Kim, K. A Roadmap for Graphene. *Nature* **2012**, *490*, 192–200.
- Schwierz, F. Graphene Transistors. *Nat. Nanotechnol.* **2010**, *5*, 487–496.
- Li, X.; Wang, X.; Zhang, L.; Lee, S.; Dai, H. Chemically Derived, Ultrasmooth Graphene Nanoribbon Semiconductors. *Science* **2008**, *319*, 1229–1232.
- Son, Y.-W.; Cohen, M. L.; Louie, S. G. Energy Gaps in Graphene Nanoribbons. *Phys. Rev. Lett.* **2006**, *97*, 216803.
- Han, M. Y.; Ozylmaz, B.; Zhang, Y.; Kim, P. Energy Band-Gap Engineering of Graphene Nanoribbons. *Phys. Rev. Lett.* **2007**, *98*, 206805.
- Kato, T.; Hatakeyama, R. Site-and Alignment-Controlled Growth of Graphene Nanoribbons from Nickel Nanobars. *Nat. Nanotechnol.* **2012**, *7*, 651–656.
- Jiao, L.; Wang, X.; Diankov, G.; Wang, H.; Dai, H. Facile Synthesis of High-Quality Graphene Nanoribbons. *Nat. Nanotechnol.* **2010**, *5*, 321–325.
- Kosynkin, D. V.; Higginbotham, A. L.; Sinteskii, A.; Lomeda, J. R.; Dimiev, A.; Price, B. K.; Tour, J. M. Longitudinal Unzipping of Carbon Nanotubes to Form Graphene Nanoribbons. *Nature* **2009**, *458*, 872–876.
- Jiao, L.; Zhang, L.; Wang, X.; Diankov, G.; Dai, H. Narrow Graphene Nanoribbons from Carbon Nanotubes. *Nature* **2009**, *458*, 877–880.
- Martin-Fernandez, I.; Wang, D.; Zhang, Y. Direct Growth of Graphene Nanoribbons for Large-Scale Device Fabrication. *Nano Lett.* **2012**, *12*, 6175–6179.
- Sprinkle, M.; Ruan, M.; Hu, Y.; Hankinson, J.; Rubio-Roy, M.; Zhang, B.; Wu, X.; Berger, C.; de Heer, W. A. Scalable Templated Growth of Graphene Nanoribbons on SiC. *Nat. Nanotechnol.* **2010**, *5*, 727–731.
- De Heer, W. A.; Berger, C.; Ruan, M.; Sprinkle, M.; Li, X.; Hu, Y.; Zhang, B.; Hankinson, J.; Conrad, E. Large Area and Structured Epitaxial Graphene Produced by Confinement Controlled Sublimation of Silicon Carbide. *Proc. Natl. Acad. Sci. U. S. A.* **2011**, *108*, 16900–16905.
- Baringhaus, J.; Ruan, M.; Edler, F.; Tejeda, A.; Sicot, M.; Taleb-Ibrahimi, A.; Li, A.-P.; Jiang, Z.; Conrad, E. H.; Berger, C., Exceptional ballistic transport in epitaxial graphene nanoribbons. *Nature* **2014**, *506*, 349–354.
- Sokolov, A. N.; Yap, F. L.; Liu, N.; Kim, K.; Ci, L.; Johnson, O. B.; Wang, H.; Vosgueritchian, M.; Koh, A. L.; Chen, J. Direct Growth of Aligned Graphitic Nanoribbons from a DNA Template by Chemical Vapour Deposition. *Nat. Commun.* **2013**, *4*, 2402, DOI: 10.1038/ncomms3402.
- Liu, N.; Kim, K.; Hsu, P.-C.; Sokolov, A. N.; Yap, F. L.; Yuan, H.; Xie, Y.; Yan, H.; Cui, Y.; Hwang, H. Y., Large-Scale Production of Graphene Nanoribbons from Electrospun Polymers. *J. Am. Chem. Soc.* **2014**, *136*, 17284–17291.
- Huang, Z.-M.; Zhang, Y. Z.; Kotaki, M.; Ramakrishna, S. A Review on Polymer Nanofibers by Electrospinning and Their Applications in Nanocomposites. *Compos. Sci. Technol.* **2003**, *63*, 2223–2253.
- Greiner, A.; Wendorff, J. H. Electrospinning: A Fascinating Method for the Preparation of Ultrathin Fibres. *Angew. Chem., Int. Ed.* **2007**, *46*, 5670–5703.
- Li, D.; Xia, Y. Electrospinning of Nanofibers: Reinventing the Wheel? *Adv. Mater.* **2004**, *16*, 1151–1170.
- Filik, J.; May, P.; Pearce, S.; Wild, R.; Hallam, K. XPS and Laser Raman Analysis of Hydrogenated Amorphous Carbon Films. *Diamond Relat. Mater.* **2003**, *12*, 974–978.
- Jackson, S. T.; Nuzzo, R. G. Determining Hybridization Differences for Amorphous Carbon from the XPS C 1s Envelope. *Appl. Surf. Sci.* **1995**, *90*, 195–203.
- Smilgies, D.-M. Scherrer Grain-Size Analysis Adapted to Grazing-Incidence Scattering with Area Detectors. *J. Appl. Crystallogr.* **2009**, *42*, 1030–1034.
- Boulch, F.; Schouler, M.-c.; Donnadieu, P.; Chaix, J.-M.; Djurado, E. *Image Anal. Stereol.* **2001**, *20*, 157–161.
- Olshavsky, M.; Goldstein, A.; Alivisatos, A. Organometallic Synthesis of Gallium-Arsenide Crystallites, Exhibiting Quantum Confinement. *J. Am. Chem. Soc.* **1990**, *112*, 9438–9439.
- Cançado, L. G.; Jorio, A.; Ferreira, E. H. M.; Stavale, F.; Achete, C. A.; Capaz, R. B.; Moutinho, M. V. O.; Lombardo, A.; Kulmala, T. S.; Ferrari, A. C. Quantifying Defects in Graphene via Raman Spectroscopy at Different Excitation Energies. *Nano Lett.* **2011**, *11*, 3190–3196.
- Tuinstra, F.; Koenig, J. L. Raman Spectrum of Graphite. *J. Chem. Phys.* **1970**, *53*, 1126–1130.
- Ferrari, A.; Robertson, J. Interpretation of Raman Spectra of Disordered and Amorphous Carbon. *Phys. Rev. B: Condens. Matter Mater. Phys.* **2000**, *61*, 14095.
- Mattia, D.; Rossi, M.; Kim, B.; Korneva, G.; Bau, H.; Gogotsi, Y. Effect of Graphitization on the Wettability and Electrical Conductivity of CVD-Carbon Nanotubes and Films. *J. Phys. Chem. B* **2006**, *110*, 9850–9855.
- Maitra, T.; Sharma, S.; Srivastava, A.; Cho, Y.-K.; Madou, M.; Sharma, A. Improved Graphitization and Electrical Conductivity of Suspended Carbon Nanofibers Derived from Carbon Nanotube/Polyacrylonitrile Composites by Directed Electrospinning. *Carbon* **2012**, *50*, 1753–1761.